Article

Divergent Oxidative Rearrangements in Solution and in a Zeolite: Distal vs Proximal Bond Cleavage of Methylenecyclopropanes

Hiroshi Ikeda, Tsuyoshi Nomura, Kimio Akiyama, Mitsuhiro Oshima, Heinz D. Roth, Shozo Tero-Kubota, and Tsutomu Miyashi

J. Am. Chem. Soc., **2005**, 127 (41), 14497-14504• DOI: 10.1021/ja045930n • Publication Date (Web): 17 September 2005

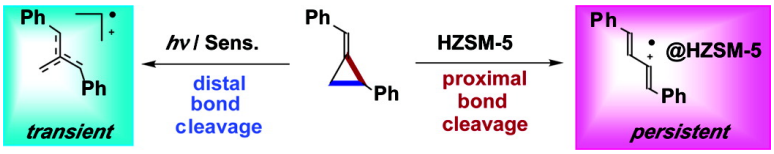

More About This Article

Additional resources and features associated with this article are available within the HTML version:

- Supporting Information
- Access to high resolution figures
- Links to articles and content related to this article
- Copyright permission to reproduce figures and/or text from this article

View the Full Text HTML

J|A|C|S
ARTICLES
Published on Web 09/17/2005

Divergent Oxidative Rearrangements in Solution and in a Zeolite: Distal vs Proximal Bond Cleavage of Methylenecyclopropanes

Hiroshi Ikeda,*,† Tsuyoshi Nomura,† Kimio Akiyama,§ Mitsuhiro Oshima,† Heinz D. Roth,*,‡ Shozo Tero-Kubota,§ and Tsutomu Miyashi†

Contribution from the Department of Chemistry, Graduate School of Science, Tohoku University, Sendai 980-8578, Japan, Institute of Multidisciplinary Research for Advanced Materials, Tohoku University, Sendai 980-8577, Japan, and Department of Chemistry and Chemical Biology, Rutgers University, Wright-Rieman Laboratories, New Brunswick, New Jersey 08854-8087

Received July 8, 2004; E-mail: ikeda@org.chem.tohoku.ac.jp; roth@rutchem.rutgers.edu

Abstract: Irradiation of 9,10-dicyanoanthracene (DCA) or *p*-chloranil in the presence of *E*-1-benzylidene-2-phenylcyclopropane (*E*-**5**) in CH_2Cl_2 causes *E*-**5** to undergo methylenecyclopropane rearrangement. An adduct, *Z*-**7**, between DCA and **5** firmly supports the involvement of a bifunctional trimethylenemethane radical cation. In contrast, incorporation of *E*-**5** into HZSM-5 produces *trans*,*trans*-1,4-diphenyl-1,3-butadiene radical cation sequestered in the HZSM-5 interior, *tt*-**8**$^{\bullet+}$@HZSM-5, identified by ESR and diffuse reflectance spectroscopy. In addition, low yields of *tt*-**8**, its *cis*,*trans*-isomer (*ct*-**8**), and 1-phenyl-1,2-dihydronaphthalene (**9**) were isolated from the supernatant solution. The sharp contrast between the photoinduced electron-transfer reaction with photosensitizers in solution and the spontaneous reaction with redox-active acidic zeolite offers the prospect of further zeolite-induced regiodivergent reactions in a range of additional substrates.

Introduction

The thermal rearrangement of methylenecyclopropane (MCP) systems and the underlying mechanism have been investigated in detail,[1] as has the nature of the related trimethylenemethane (TMM), one of the most thoroughly investigated diradical systems.[2] Subsequently, the developing interest in electron transfer and radical ion chemistry caused the structures and reactivities of suitable MCP radical cations to be scrutinized.[3] For example, electron transfer (ET) from 1,1-dianisyl-2-methylenecyclopropane (**1**, Scheme 1) to triplet *p*-chloranil (CA) generates a bifunctional TMM radical cation, **2**$^{\bullet+}$; CIDNP effects observed during this reaction showed that the unpaired electron spin density and the charge of **2**$^{\bullet+}$ are residing in separate

Scheme 1 [a]

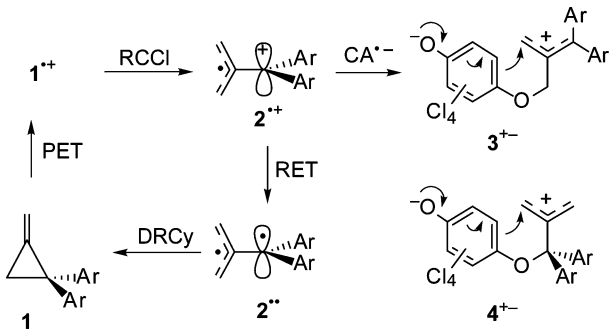

[a] Ar; anisyl.

π-systems, the spin in the allyl group, and the charge in the diphenylmethylene function.[3b] The limited delocalization of spin and charge is due to the attachment of the diphenylmethylene moiety in the node of the allyl function; the two π-systems need not be orthogonal, as initially suggested.[3a,b] The radical cation, **2**$^{\bullet+}$, forms two spiro-annelated CA-adducts[3b] via zwitterions, **3**$^{+-}$ and **4**$^{+-}$,[4] formed by coupling of singlet ion pairs, and regenerates the starting material, **1**. Recent spectroscopic studies, using time-resolved absorption and ESR spectroscopy and photoacoustic calorimetry following nanosecond laser flash photolysis support the intermediacy of a triplet biradical, **2**$^{\bullet\bullet}$, formed by triplet return (R) ET.[3c,d] In summary, the photoinduced (P) ET MCP rearrangement of **1** proceeds in three stages: radical cation cleavage (RCCl), triplet RET, and

* To whom correspondence should be addressed.
† Graduate School of Science, Tohoku University.
‡ Institute of Multidisciplinary Research for Advanced Materials, Tohoku University.
§ Rutgers University.

(1) (a) Ullman, E. F. *J. Am. Chem. Soc.* **1960**, *82*, 505−506. (b) Chesick, J. P. *J. Am. Chem. Soc.* **1963**, *85*, 2720−2723. (c) Doering, W. v. E.; Roth, H. D. *Tetrahedron* **1970**, *26*, 2825−2835. (d) Gajewski, J. J. *J. Am. Chem. Soc.* **1971**, *93*, 4450−4458.
(2) (a) Dowd, P. *J. Am. Chem. Soc.* **1966**, *88*, 2587−2589. (b) Dowd, P.; Chow, M. *J. Am. Chem. Soc.* **1977**, *99*, 6438−6440. (c) Dowd, P. *Acc. Chem. Res.* **1972**, *5*, 242−248. (d) Berson, J. A.; Bushby, R. J.; McBride, J. M.; Tremelling, M. *J. Am. Chem. Soc.* **1971**, *93*, 1544−1546.
(3) (a) Takahashi, Y.; Miyashi, T.; Mukai, T. *J. Am. Chem. Soc.* **1983**, *105*, 6511−6513. (b) Miyashi, T.; Takahashi, Y.; Mukai, T.; Roth, H. D.; Schilling, M. L. M. *J. Am. Chem. Soc.* **1985**, *107*, 1079−1080. (c) Ikeda, H.; Nakamura, T.; Miyashi, T.; Goodman, J. L.; Akiyama, K.; Tero-Kubota, S.; Houman, A.; Wayner, D. D. M. *J. Am. Chem. Soc.* **1998**, *120*, 5832−5833. (d) Ikeda, H.; Akiyama, K.; Takahashi, Y.; Nakamura, T.; Ishizaki, S.; Shiratori, Y.; Ohaku, H.; Goodman, J. L.; Houmam, A.; Wayner, D. D. M.; Tero-Kubota, S.; Miyashi, T. *J. Am. Chem. Soc.* **2003**, *125*, 9147−9157.
(4) (a) Roth, H. D. *J. Photochem. Photobiol., C* **2001**, *2*, 93−116. (b) Roth, H. D. *Pure Appl. Chem.* **2005**, *77*, 1075−1085.

diradical cyclization (DRCy; Scheme 1); all steps have been firmly established.

The catalytic properties of zeolites and their redox and acid−base reactivities have been investigated extensively, and a wide range of chemical reactions has been studied on the surface and in the micropores of these materials.[5] Interestingly, the nearly cylindrical channels [internal diameter (ID) ∼5.5 Å] of pentasil zeolite (HZSM-5) can generate π-type radical cations from suitable substrates at ambient temperatures.[6] The supramolecular interaction with the rigid anisotropic microporous framework stabilizes the otherwise highly reactive radical cations due to the combined effects of (a) the intense electrostatic fields inside zeolite pores, (b) topological restrictions that prevent the access of external reagents, and (c) the limiting dimensions of the zeolite channels, restricting the shape of the enclosed species.[7−9] Because of dramatically increased lifetimes (days to years at room temperature), the sequestered radical cations can be studied by conventional spectroscopic techniques.[6,10]

The dual reactivity of HZSM-5, i.e., its ability to function as an acid−base catalyst as well as a redox agent, offers the intriguing prospect that incorporation of an MCP system may lead to a selective bond cleavage differing from that occurring in homogeneous, isotropic media. Such regiodivergent reactions might be of significant value. On the other hand, the dual reactivity of HZSM-5 complicates the potential mechanisms of zeolite-induced reactions. Accordingly, few systems have been found that show contrasting ET reactivity in solution vs in a zeolite.[8,11] To examine a potentially medium-dependent regioselective bond cleavage, we studied the reactions of *E*-1-benzylidene-2-phenylcyclopropane (*E*-**5**, smallest molecular diameter = 5.5 Å) with ET photosensitizers, 9,10-dicyanoanthracene (DCA) or CA, and its spontaneous reaction upon incorporation into the redox-active acidic zeolite, HZSM-5. Our results illustrate divergent reactions for the DCA-sensitized and the HZSM-5-induced reactions of *E*-**5**; the homogeneous solution was found to promote distal bond cleavage and an MCP rearrangement, whereas the heterogeneous medium causes proximal bond cleavage (Scheme 2).

Experimental Section

Preparation of Organic Materials. Substrate *E*-**5** was obtained in 50% yield together with its geometric isomer, *Z*-**5** (16%), by oxidation of dibenzylidenemethane dianion, generated from 1,1-dibenzylethylene, according to literature procedures.[12] See the Supporting Information for physical data of *E*-**5**, *Z*-**5**, and related compounds. The anodic oxidation potential of *E*-**5** (E^{ox}_{ap} = +1.62 V vs SCE) is sufficiently low to quench excited singlet DCA at nearly the diffusion-controlled rate in CH_2Cl_2 ($k_q = 1.0 \times 10^{10}$ M^{-1} s^{-1}). Oxidation potentials (E^{ox}_{ap}), free energy changes (ΔG_{et}), and k_q for ET from *E*-**5** and related donors to singlet-excited DCA are summarized in Table 1.

Scheme 2

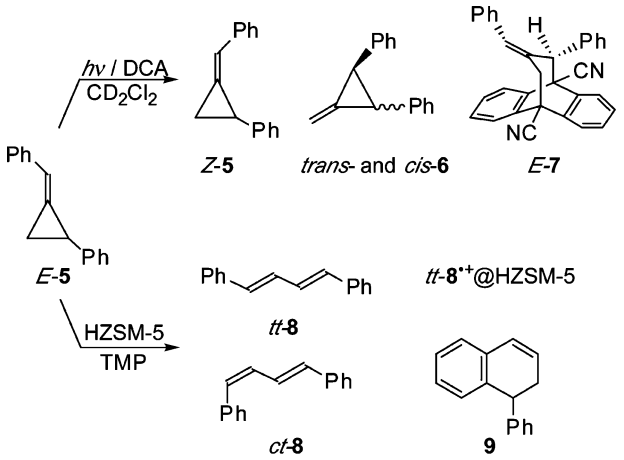

Table 1. E^{ox}_{ap}, ΔG_{et} of ET to ^{1}DCA*, and k_q for DCA Fluorescence Quenching in CH_2Cl_2 for Selected Donors

substrate	E^{ox}_{ap}[a] V	ΔG_{et}[b] eV	k_q 10^{10} M^{-1} s^{-1}
E-**5**	+1.62	−0.62	1.0
Z-**5**	+1.71	−0.53	0.78
trans-**6**	+1.51	−0.73	0.76
tt-**8**	+1.37	*c*	*c*

[a] In CH_2Cl_2 containing 0.1 M *n*-Bu_4NClO_4. [b] $\Delta G_{et} = E^{ox}_{1/2} - E^{red}$(DCA) − $^1E^*$(DCA) − $e^2/\epsilon r$.[13] $E^{ox}_{1/2} = E^{ox}_{ap}$ − 0.03 V; $E^{red}_{1/2}$(DCA) = −0.89 V vs SCE; $^1E^*$(DCA) = 2.87 eV in CH_2Cl_2. The coulomb term ($e^2/\epsilon r$) is 0.23 eV in CH_2Cl_2. [c] Not relevant to this study.

General Procedure for the DCA-Sensitized Photoreactions. Solutions containing 0.05 mmol each of a substrate and DCA in 0.5 mL of CD_2Cl_2 in Pyrex tubes (0.5 cm ID) were degassed by five freeze−pump−thaw cycles (77 K; 10^{-2} Torr; ambient temperature) and sealed at 10^{-2} Torr. The samples, containing a slight suspension of DCA, were irradiated with the output of a 2 kW Xe lamp through a cutoff filter (λ > 360 nm) at 20 ± 1 °C. Product yields were determined by ^{1}H NMR analyses. Details of product analysis and physical data of the photoproducts are shown in the Supporting Information.

Preparation of the Zeolite. Pentasil zeolites (HZSM-5; Si/Al ratio 20, 34) were obtained by calcination (500 °C, 10 h) of corresponding samples of NH_4ZSM-5 (TOSOH). The electron-accepting ability of these HZSM-5 samples and of NaZSM-5 (TOSOH, Si/Al = 11.8, similarly calcined) was examined by mixing with 2,2,4-trimethylpentane (TMP) solutions of π-type electron donors; these were inspected visually for coloration and examined by ESR spectroscopy.[6a,14] The HZSM-5 sample with Si/Al = 20 was the most powerful oxidizer with an estimated reduction potential (E^{red}_{ap}) of ∼+1.65 V vs SCE; this sample was used to probe the reactions of *E*-**5**.

General Adsorption Procedure onto the Zeolite. The substrates (1.05 mg in 10 mL anhydrous TMP) were adsorbed onto pentasil zeolite by stirring with 300 mg HZSM-5 for 2 h at room temperature. The loaded zeolite was collected by filtration, washed with dry TMP to remove material adsorbed on the surface, and dried at reduced pressure

(5) (a) Rabo, J. A., Ed. *Zeolite Chemistry and Catalysis*; ACS Monograph: 1976; Vol. 171. (b) Stucky, G. D., Dwyer, F. D., Eds. *Intrazeolite Chemistry*; ACS Monograph: 1983; Vol. 218. (c) Derouane, E. G., Lemos, F., Naccache, C., Rebeiro, F. R., Eds. *Zeolite Microporous Solids: Synthesis, Structure, and Reactivity*; Kluwer Academics: Dordrecht, 1991.
(6) (a) Ramamurthy, V.; Casper, J. V.; Corbin, D. R. *J. Am. Chem. Soc.* **1991**, *113*, 594−600. (b) Casper, J. V.; Ramamurthy, V.; Corbin, D. R. *J. Am. Chem. Soc.* **1991**, *113*, 600−610. (c) Liu, X.; Iu, K.-K.; Thomas, J. K.; He, H.; Klinowski, J. *J. Am. Chem. Soc.* **1994**, *116*, 11811−11818. (d) García, H.; Roth, H. D. *Chem. Rev.* **2002**, *102*, 3947−4007.
(7) (a) Lakkaraju, P. S.; Zhou, D.; Roth, H. D. *J. Chem. Soc., Perkin Trans. 2* **1998**, 1119−1121. (b) Martí, V.; Fernández, L.; Fornés, V.; García, H.; Roth H. D. *J. Chem. Soc., Perkin Trans. 2* **1999**, 145−152.
(8) Herbertz, T.; Lakkaraju, P. S.; Blume, F.; Blume, M.; Roth, H. D. *Eur. J. Org. Chem.* **2000**, 467−472.
(9) (a) Hirano, T.; Li, W.; Abrams, L.; Krusic, P. J.; Ottaviani, M. F.; Turro, N. J. *J. Org. Chem.* **2000**, *65*, 1319−1330. (b) Turro, N. J. *Acc. Chem. Res.* **2000**, *33*, 637−646.
(10) Vaidyalingam, A. S.; Coutant, M. A.; Dutta, P. K. In *Electron Transfer in Chemistry*; Balzani, V., Ed.; Wiley: Weinheim, 2001; Vol. 4, pp 412−486.
(11) For example, see: (a) Kojima, M.; Takeya, H.; Kuriyama, Y.; Oishi, S. *Chem. Lett.* **1997**, 997−998. (b) Roth, H. D.; Herbertz, T.; Lakkaraju, P. S.; Sluggett, G.; Turro, N. J. *J. Phys. Chem. A* **1999**, *103*, 11350−11354. (c) Ikeda, H.; Minegishi, T.; Miyashi, T.; Lakkaraju, P. S.; Sauers, R. R.; Roth, H. D. *J. Phys. Chem. B* **2005**, *109*, 2504−2511.
(12) Witt, O.; Mauser, H.; Friedl, T.; Wilhelm, D.; Clark, T. *J. Org. Chem.* **1998**, *63*, 959−967.
(13) Rehm, D.; Weller, A. *Isr. J. Chem.* **1970**, *8*, 259−271.
(14) See the Supporting Information for details.

(≤1 Torr). For product analysis, 30 mg of *E*-**5** (0.15 mmol) and 8.0 g of HZSM-5 were stirred at room temperature for 5 h. After filtration on a sintered glass disk, the loaded, colored zeolite was washed with TMP. After removing the solvent from the filtrate the products were separated by preparative HPLC; structures and yields were determined by 200 MHz ^{1}H NMR analysis. Physical data of the products obtained in the zeolite-catalyzed reactions are shown in the Supporting Information.

***γ*-Irradiation of Glassy Matrices.** *n*-BuCl solutions (1 mL) of the substrates (10 mM) in a flat quartz cell (2 × 10 × 40 mm) were degassed by five freeze−pump−thaw cycles (77 K; 10^{-2} Torr; ambient temperature) and sealed at 10^{-2} Torr. A glassy matrix was obtained by steeping the cell into liquid nitrogen. This cell was irradiated with a 5.1 TBq ^{60}Co source in liquid nitrogen at 77 K for 40 h. The absorption spectra before and after irradiation were recorded at 77 K.

ESR Studies. ESR spectra of the dried zeolite samples were recorded on an X-band spectrometer (9.3 GHz) in the CW mode. Typically, a single scan gave a satisfactory spectrum; the spectra reproduced in the figures were accumulations of eight scans. Details of the CIDEP experiments have been described in the Supporting Information of refs 3d and 15.

Quantum Chemical Calculations. Density functional theory (DFT) and TD-DFT calculations for key radical cations were carried out with the Gaussian 98 suite of electronic structure programs using extended basis sets, including d-type polarization functions on carbon.[16] The geometries of the radical cations were optimized at the unrestricted B3LYP[17] level with the standard 6-31G** basis set.

Results

Photoinduced Reaction of *E*-5. Irradiation (2 kW Xe lamp, $\lambda > 360$ nm) of DCA ($^1E^* = 2.87$ eV; $E^{red}_{1/2} = -0.89$ V vs SCE in CH_2Cl_2) in degassed CH_2Cl_2 in the presence of *E*-**5** ($E^{ox}_{ap} = +1.62$ V vs SCE) for 15 min led to the formation of the geometric isomer *Z*-**5**, as well as two structural isomers, *cis*-**6** and *trans*-**6**, in 9, 13, and 33% yield, respectively, after 1 h. In addition, a DCA-adduct, *Z*-**7**, was formed (Scheme 2; Figure 1, top). The figure clearly shows three phases in the photoreaction. In the earliest phase, *E*-**5** is rapidly depleted and *trans*-**6** is built up, along with *cis*-**6** and *Z*-**5**; *trans*-**6** reaches a maximum at ∼15 min. In the second phase, *trans*-**6** is depleted in favor of *cis*-**6** and *Z*-**5**; these products show near-plateaus between 30 and 90 min. Finally, continued irradiation causes the three isomers, *Z*-**5**, *cis*-**6**, and *trans*-**6** to be depleted in favor of the adduct *Z*-**7**, which became the predominant product after 4 h irradiation. Similar results were observed during the reaction of DCA with *E*-**5** in DMSO-d_6.

The photoinduced reaction of the geometric isomer, *Z*-**5**, with DCA under otherwise identical conditions also gave rise to *cis*- and *trans*-**6** as well as the adduct *Z*-**7**. The significant difference to the reaction of *E*-**5** lies in the observation that the rise of adduct *Z*-**7** does not show an "induction period" but occurs without delay (Figure 1, bottom).

To probe the nature of the radical cation intermediate, CA ($^3E^* = 2.7$ eV; $E^{red}_{1/2} = +0.02$ V vs SCE) was irradiated (355 nm) in DMSO in the presence of *E*-**5** at ambient temperature in an ESR cavity. This reaction gave rise to a CIDEP spectrum[18] featuring an intense emission signal at $H = 3365$ G ($g =$ 2.0058), assigned to the tetrachlorobenzosemiquinone radical anion ($CA^{\bullet-}$)[20] and a weak, complex emission signal at $H =$ 3350−3400 G ($g \sim 2.002$) due to (a) species arising from *E*-**5** (Figure 2, bottom).

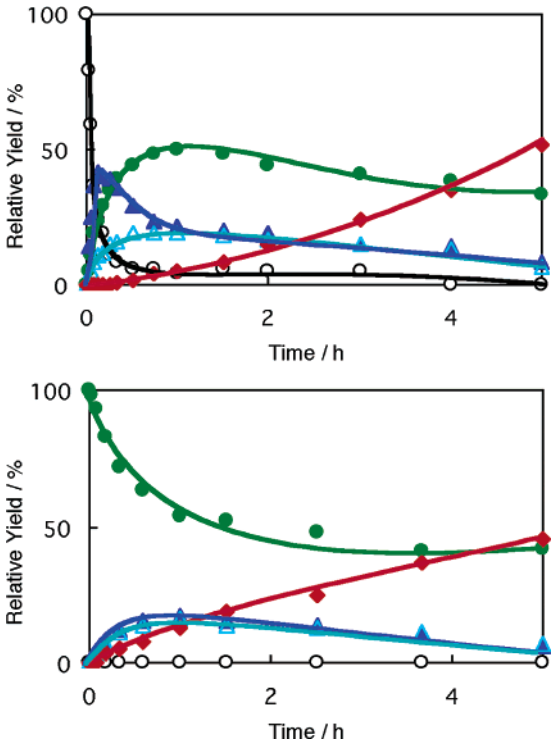

Figure 1. Product distribution obtained upon irradiation of DCA in degassed CH_2Cl_2 in the presence of *E*-**5** (top: black circles) or *Z*-**5** (bottom; green filled circles) as a function of time: *trans*-**6** (blue triangles), *cis*-**6** (light blue triangles), and *Z*-**7** (red filled diamonds).

Zeolite-Induced Reactions. The interaction of *E*-**5** with HZSM-5 produced significantly different results. Upon stirring a suspension of HZSM-5 (Si/Al = 20, 300 mg) in TMP containing *E*-**5** (5 μmol) for 8 h, three products were isolated from the supernatant liquid: *trans*,*trans*- and *cis*,*trans*-1,4-diphenyl-1,3-butadiene (*tt*-**8** and *ct*-**8**) and 1-phenyl-1,2-dihydronaphthalene (**9**, Scheme 2) in 10, 3, and 10% yield, respectively. In addition, 65% of *E*-**5** was incorporated into the zeolite, giving it a pink hue.

An ESR spectrum (Figure 3, top) of the dried pink zeolite was persistent at room temperature; this spectrum was identified as that of *tt*-**8**$^{\bullet+}$@HZSM-5, because it is essentially identical with one obtained from authentic *tt*-**8** upon incorporation into HZSM-5.[6a,14] Furthermore, the diffuse reflectance (DR) spectrum of the pink zeolite sample obtained upon incorporation of *E*-**5** was identical with the DR spectrum observed upon incorporation of *tt*-**8** (Figure 4, top), further supporting the identification of the sequestered ion and confirming the HZSM-5-catalyzed isomerization of *E*-**5** to *tt*-**8**$^{\bullet+}$@HZSM-5.

(15) (a) Akiyama, K.; Tero-Kubota, S.; Ikegami, Y.; Ikenoue, T. *J. Am. Chem. Soc.* **1984**, *106*, 8322−8323. (b) Akiyama, K.; Tero-Kubota, S.; Ikoma, T.; Ikegami, Y. *J. Am. Chem. Soc.* **1994**, *116*, 5324−5327.
(16) Frisch, M. J. et al. *Gaussian 98*, revision A.11.4; Gaussian Inc.; Pittsburgh, PA, 1998.
(17) (a) Becke, A. D. *J. Chem. Phys.* **1993**, *98*, 5648−5652. (b) Lee, C.; Yang, W.; Parr, R. G. *Phys. Rev. B* **1988**, *37*, 785−789.
(18) For recent CIDEP studies on PET reactions of organic substrates, see ref 3d and 19.
(19) (a) Ishiguro, K.; Khudyakov, I. V.; McGarry, P. F.; Turro, N. J.; Roth, H. D. *J. Am. Chem. Soc.* **1994**, *116*, 6933−6934. (b) Kobori, Y.; Yago, T.; Akiyama, K.; Tero-Kubota, S. *J. Am. Chem. Soc.* **2001**, *123*, 9722−9723. (c) Akiyama, K.; Tero-Kubota, S. *J. Phys. Chem. B* **2002**, *106*, 2398−2403. (d) Yago, T.; Kobori, Y.; Akiyama, K.; Tero-Kubota, S. *J. Phys. Chem. B* **2003**, *107*, 13255−13257. (e) Kobori, Y.; Yago, T.; Akiyama, K.; Tero-Kubota, S.; Sato, H.; Hirata, F.; Norris, J. R., Jr. *J. Phys. Chem. B* **2004**, *108*, 10226−10240.
(20) Segal, B. G.; Kaplan, M.; Fraenkel, G. K. *J. Chem. Phys.* **1965**, *43*, 4191−4200.

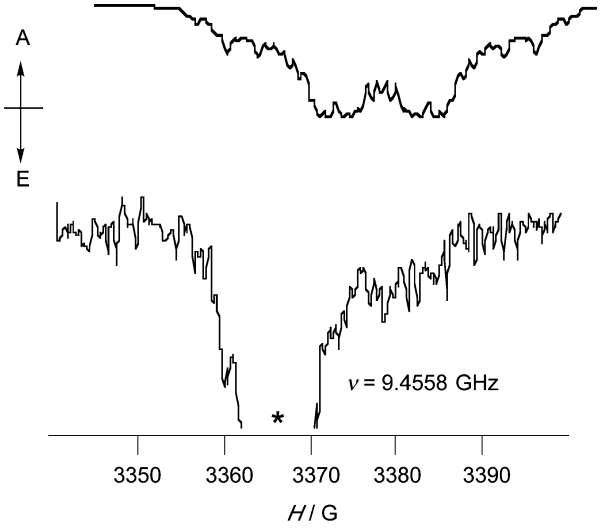

Figure 2. CIDEP spectrum observed at a delay time of 500 ns after the laser excitation of CA in the presence of *E*-**5** in DMSO (bottom); the asterisk (*) represents emission due to $CA^{\bullet-}$. A simulated spectrum with hyperfine coupling constants (a_H) of bifunctional radical cation, *E*-$\mathbf{10}^{\bullet+}$ (see text), is shown above.

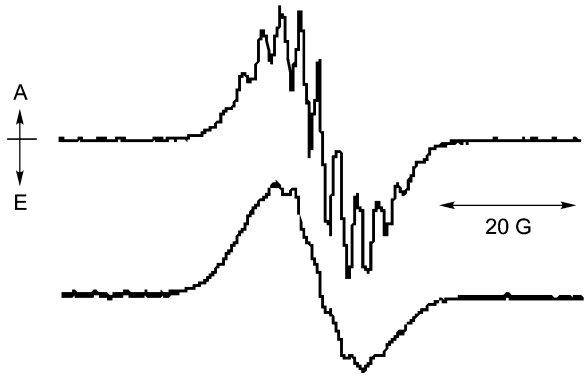

Figure 3. (Top) Steady-state CW-ESR spectra of *tt*-$\mathbf{8}^{\bullet+}$@HZSM-5 (g = 2.0023, line width = 0.8 G) obtained upon inclusion of *E*-**5** in HZSM-5 at room temperature and (bottom) of *tt*-$\mathbf{8}^{\bullet+}$ (g = 2.0023, line width = 2.3 G) obtained upon γ-irradiation in an *n*-BuCl matrix at 77 K.

ESR and absorption spectra of *tt*-$\mathbf{8}^{\bullet+}$ were also obtained upon γ-ray irradiation of *tt*-**8** in a glassy matrix (*n*-butyl chloride, *n*-BuCl) at 77 K. In the *n*-BuCl matrix the absorption maximum (548 and 822 nm, Figure 4, bottom) is slightly red-shifted relative to the DR spectrum in the zeolite (540 and 817 nm). Similar γ-irradiation of *E*-**5** gave a weak 446-nm band, but not the 548- and 822-nm bands. The ESR signals of *tt*-$\mathbf{8}^{\bullet+}$@HZSM-5 were noticeably sharper than those of *tt*-$\mathbf{8}^{\bullet+}$ in the frozen *n*-BuCl matrix (Figure 3, bottom).

The geometric isomer, *Z*-**5**, was also allowed to interact with HZSM-5 under the same conditions as the *E*-isomer; this reaction gave rise to *tt*- and *ct*-**8**, **9**, in the supernatant liquid and also resulted in the pink *tt*-$\mathbf{8}^{\bullet+}$@HZSM-5.

In contrast, a bulkier analogue of *E*-**5**, *E*-1-[(3,5-dimethylphenyl)methylene]-2-(3,5-dimethylphenyl)cyclopropane, *E*-**11**, whose smallest molecular diameter (~7 Å) is significantly larger than the pore size of HZSM-5, gave rise to the corresponding 1,3-butadiene (*tt*- and *ct*-**12**) and 1,2-dihydronaphthalene (**13**) derivatives (Scheme 3) but failed to produce any perceptible color on the surface (or inside) of the zeolite sample.

Quantitative Adsorption Experiments with *E*-5. To gain further insight into the formation of *tt*-$\mathbf{8}^{\bullet+}$@HZSM-5 from *E*-**5** on HZSM-5, we conducted quantitative adsorption experiments. Based on the quantities of holes of straight channels (N_h) and active sites (N_s) of HZSM-5 and the molecular volume of *tt*-$\mathbf{8}^{\bullet+}$@HZSM-5 we estimated the occupation of holes and active sites. For 100 mg of HZSM-5, N_h and N_s were estimated to be 0.082 and 33 μmol, respectively (Table 2). The value of N_h was determined by an N_2 gas absorption experiment; a calculation based on an SEM image of HZSM-5 gave a similar value (0.11 μmol for 100 mg of HZSM-5). The N_s values are based on the experimentally determined micropore volume of the straight channels (9.2×10^{-8} m^3/unit cell), the molecular volume of one *tt*-$\mathbf{8}^{\bullet+}$ molecule (4.9×10^{-28} m^3), and the assumption that (a) the rigid *tt*-$\mathbf{8}^{\bullet+}$ molecules can be adsorbed in the straight, but not the zigzag channels of HZSM-5, and (b) one unit cell of HZSM-5 (19.9 Å length along a zigzag channel) can adsorb two *tt*-$\mathbf{8}^{\bullet+}$ molecules (14 Å length) because one unit cell of the HZSM-5 has two straight channels. A similar N_s value (37 μmol per 100 mg HZSM-5) was calculated from the absorption volume per gram. Accordingly, each channel of HZSM-5 has ~400 sites (~33 μmol/0.083 μmol) for *tt*-$\mathbf{8}^{\bullet+}$.

The degree of conversion of *E*-**5** depended strongly on the "loading" ratio of substrate to zeolite. For example, stirring *E*-**5** (1.03 mg, 5.0 μmol) with HZSM-5 (100 mg) produced a mixture of *E*-**5**, *tt*-**8**, *ct*-**8**, and **9** in 53, 7, 2, and 5% yield, respectively

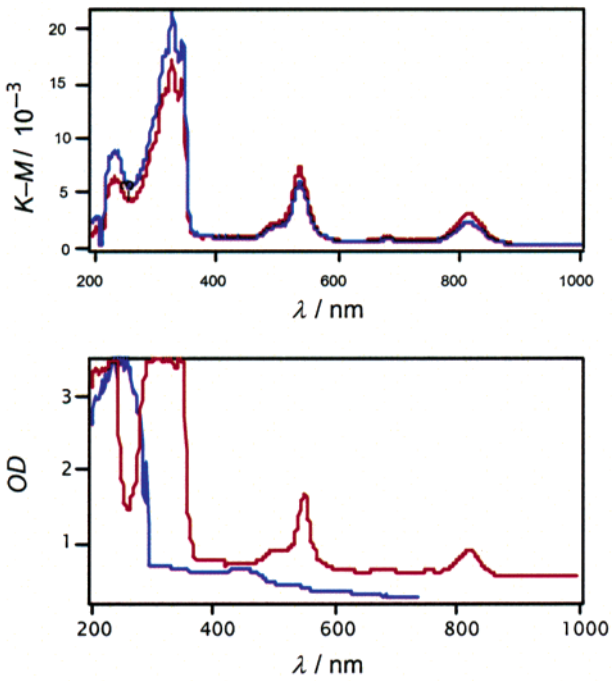

Figure 4. (Top) DR spectra, assigned to *tt*-$\mathbf{8}^{\bullet+}$, obtained by inclusion of *E*-**5** (blue) and *tt*-**8** (red) in HZSM-5 at room temperature. (Bottom) Absorption spectra observed upon γ-irradiation of an *n*-BuCl glassy matrix of *E*-**5** (blue) and *tt*-**8** (red) at 77 K; γ-irradiation of *E*-**5** does not generate *tt*-$\mathbf{8}^{\bullet+}$.

Scheme 3 [a]

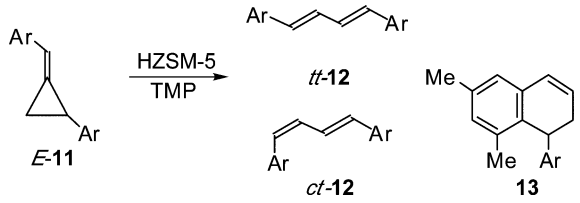

[a] Ar; 3,5-dimethylphenyl.

Table 2. Quantitative Adsorption Experiment of *E*-**5** (1.03 mg, 5.0 μmol) onto HZSM-5 for 8 h

HZSM-5 mg	N_h[a] μmol	N_s[a] μmol	yield/% *E*-**5**	*tt*-**8**	*ct*-**8**	**9**	SAD[b]	*tt*-**8**$^{\bullet+}$@HZSM-5	fraction of occupied holes	fraction of occupied sites
100	0.082	33	53	7	2	5	3	30 (1.8 μmol)	~18	~0.05
200	0.16	66	22	9	3	7	9	50 (2.5 μmol)	~15	~0.04
300	0.24	100	2	10	3	10	10	65 (3.3 μmol)	~13	~0.03

[a] Quantities of holes of straight channels (N_h) and active sites (N_s) of HZSM-5 for *tt*-**8**$^{\bullet+}$. [b] Estimated amounts of the surface adsorption and decomposition.

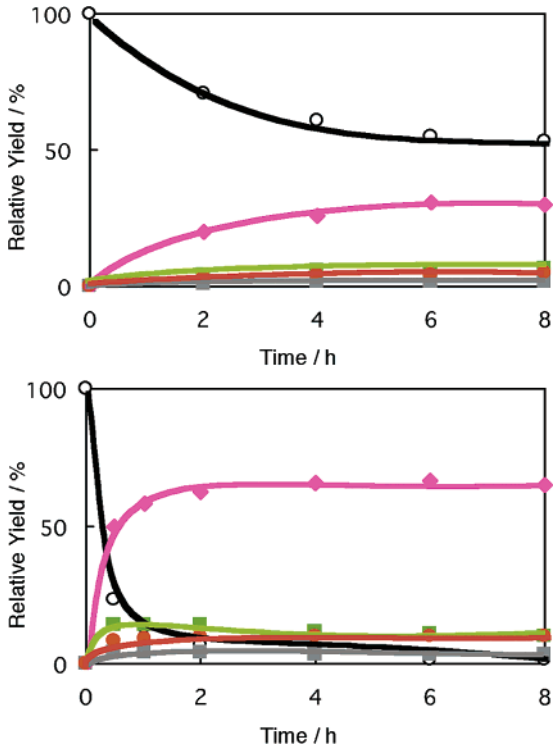

Figure 5. Time-dependent changes in the product distribution obtained by treating *E*-**5** (black circles) with 100 mg of HZSM-5 (top) and 300 mg of HZSM-5 (bottom) in TMP; *tt*-**8** (lime green filled squares), *ct*-**8** (gray filled squares), **9** (orange filled circles), and *tt*-**8**$^{\bullet+}$@HZSM-5 (pink filled diamonds).

(Table 2 and Figure 5, top). The yield and amount (30%, 1.5 μmol) of *tt*-**8**$^{\bullet+}$@HZSM-5 was determined from the yield data and the amount of surface adsorption and decomposition (3%), which was estimated from a control experiment with HZSM-5 and a bulky 1,3-butadiene, *tt*-**12**. This value indicated that about 18 molecules of *tt*-**8** (~1.5 μmol/0.082 μmol) enter a HZSM-5 channel through the same hole but that only 4.5% of the sites (~1.5 μmol/33 μmol) were occupied by *tt*-**8**$^{\bullet+}$. Thus, on the average, 18 of the 400 sites are occupied by *tt*-**8**$^{\bullet+}$ in each channel under these conditions (Figure 6). When larger amounts (200 or 300 mg) of HZSM-5 were used with the same quantity of *E*-**5**, the yield of *tt*-**8**$^{\bullet+}$@HZSM-5 increased (Figure 5, bottom) but the population of occupied holes and sites decreased accordingly (Table 2).

Discussion

The divergent results obtained in the oxidative rearrangement of the MCP system, *E*-**5**, under the different reaction conditions are incompatible with the involvement of only one intermediate; the range of products obtained can be reconciled only if at least two different intermediates are involved. The nature of the products obtained by ET in solution (Scheme 2) supports cleavage of the distal cyclopropane bond, whereas HZSM-5

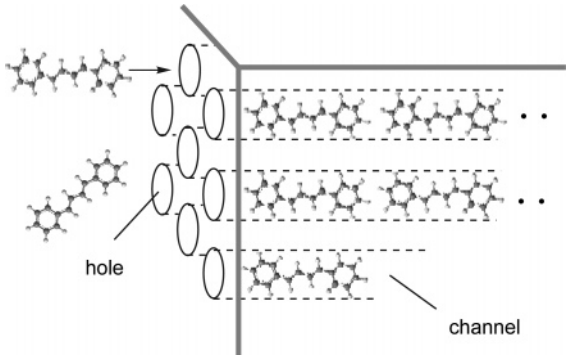

Figure 6. A model of the adsorption of *tt*-**8** into HZSM-5 zeolite, giving rise to *tt*-**8**$^{\bullet+}$@HZSM-5.

Scheme 4 [a]

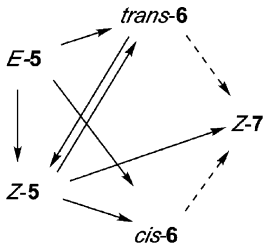

[a] Plain arrows; pathways supported by the reactions of *E*-**5** and *Z*-**5**. Dashed arrows; additional likely pathways.

apparently promotes cleavage of the proximal cyclopropane bond. The likely course of the divergent reactions is considered below.

Mechanism of the Photoinduced Reaction of *E*-5. The significantly exergonic free energy for ET from *E*-**5** to ^{1}DCA* ($\Delta G_{et} = -0.62$ eV) leaves little doubt that this photoreaction proceeds via ET. The overall mechanism must accommodate three key findings: (a) the early buildup of *trans*-**6** from *E*-**5** and the failure of the initial radical cation derived from *E*-**5** to form a DCA adduct;[21] (b) the delay of *Z*-**7** formation from *E*-**5** in contrast to the ready adduct formation from *Z*-**5**; and (c) the *Z*-stereochemistry of the adduct (*Z*-**7**).[21] The unambiguously documented conversions are summarized in Scheme 4.

The conversions between *E*- and *Z*-**5** and *cis*- and *trans*-**6** are typical MCP rearrangements. The corresponding well-documented rearrangement of the dianisyl analogue, **1**,[3] clearly proceeds via a ring-opened TMM-type radical cation formed by cleavage of the distal cyclopropane bond. In addition, **1** is known to give rise to a ring-closed as well as a ring-opened molecular ion in the gas phase.[22] It is tempting to invoke analogous ring-opened species for *E*-**5** and its isomers. On the other hand, the known persistence of ring-closed radical cations *cis*- and *trans*-**14**$^{\bullet+}$ and **15**$^{\bullet+}$ (Chart 1), derived from 1,2-

(21) For a possible formation of *E*-**7**, a stereoisomer of *Z*-**7**, from *E*-**10**$^{\bullet+}$, see the Supporting Information.
(22) Pineda, C.-J.; Roth, H. D.; Mujsce, A. M.; Schilling, M. L. M.; Reents, W. D., Jr. *J. Phys. Org. Chem.* **1989**, *2*, 117−130.

Chart 1

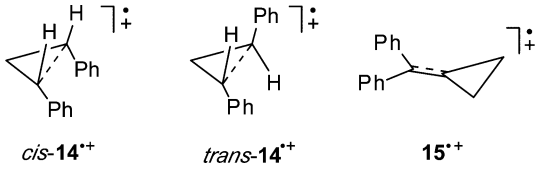

cis-**14**$^{\bullet+}$ *trans*-**14**$^{\bullet+}$ **15**$^{\bullet+}$

Scheme 5

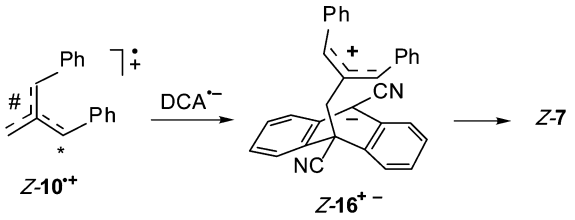

Z-**10**$^{\bullet+}$ *Z*-**16**$^{+-}$

diphenylcyclopropanes[23] and (diphenylmethylene)cyclopropane,[3b] respectively, clearly indicates that ring-closed radical cations cannot be excluded a priori. The failure of *E*-**5** to form a DCA-adduct (*Z*-**7** or an isomer) argues against a ring-opened radical cation derived from *E*-**5**$^{\bullet+}$, although its rapid conversion to *trans*-**6** may argue for a ring-opened species. Of course, the formation of the DCA-adduct *Z*-**7** provides irrefutable evidence for a ring-opened TMM-type radical cation formed by cleavage of the distal cyclopropane bond. The precedent of the PET reaction between CA and **1**[3] suggests coupling of a radical ion pair, *Z*-**10**$^{\bullet+}$−DCA$^{\bullet-}$. In further analogy, the addition likely involves coupling of singlet ion pairs with formation of zwitterion, *Z*-**16**$^{+-}$ (Scheme 5).[3]

One key to the electronic structure of the principal radical cation derived from *E*-**5**, ring-closed (*E*-**5**$^{\bullet+}$) or of the TMM-type (*E*-**10**$^{\bullet+}$), lies in the distribution of the unpaired electron spin density and of the positive charge. As mentioned earlier, **1** forms the unusual intermediate, **2**$^{\bullet+}$, in which spin and charge reside in separate π-systems. For the ring-opened radical cation derived from *E*-**5**, two limiting possibilities exist to deploy spin and charge: either between an *E*,*E*-1,3-diphenylallyl system and a methylene function attached at the nodal C-2 (*E*-**10**-A$^{\bullet+}$) or between a 1-phenylallyl system and a benzyl function attached at C-2 (*E*-**10**-B$^{\bullet+}$).

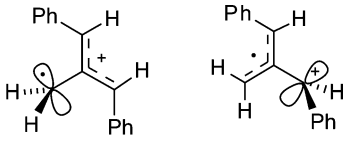

E-**10**-A$^{\bullet+}$ *E*-**10**-B$^{\bullet+}$

Density functional theory (DFT) and semiempirical calculations suggested different electronic structures for *E*-**10**$^{\bullet+}$. A UB3LYP/6-31G** calculation indicated structure *E*-**10**-A$^{\bullet+}$ with most of the unpaired spin density (71%) localized on the methylene (CH_2) carbon and the positive charge (97%) delocalized in the *E*,*E*-1,3-diphenylallyl subunit. On the other hand, the UAM1 calculation favored electronic structure *E*-**10**-B$^{\bullet+}$.

The CIDEP spectrum[18] (Figure 2, bottom) provides limited insight into the structure of *E*-**10**$^{\bullet+}$. The strong emission signal (g = 2.0058) clearly is due to CA$^{\bullet-}$.[20] The balance of the spectrum (g ~2.002) is ascribed to (a) radical cation(s) derived from *E*-**5**$^{\bullet+}$. This spectrum was partially reproduced by a spectrum simulated with the hyperfine coupling constants (hfcc, a_H) of the *Z*-1-phenylallyl radical[24] (Figure 1), suggesting the electronic structure, *E*-**10**-B$^{\bullet+}$, as shown below. However, the observed spectrum is weak and may be complicated by the presence of additional radical species.

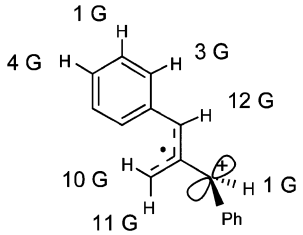

E-**10**-B$^{\bullet+}$

In summary, the true electronic structure of the principal radical cation derived from *E*-**5** and the detailed mechanism of the MCP rearrangement remain open to question. However, the combined evidence derived from product analysis, CIDEP spectrum, and calculations together with the precedent of the dianisyl derivative, **1**, support ring-opened radical cations (**10**$^{\bullet+}$), especially *Z*-**10**$^{\bullet+}$ as an incontrovertible precursor for *Z*-**7**. Our previous work on **1**[3c,d] suggests that the products may be formed via diradicals *E*-**10**$^{\bullet\bullet}$ and/or *Z*-**10**$^{\bullet\bullet}$; this aspect of the mechanism is being pursued.

Mechanism of the Zeolite-Induced Conversion of *E*-5. The alternative method applied to oxidize *E*-**5**, incorporation into HZSM-5, generated entirely different products (Scheme 2), requiring the involvement of a different intermediate formed by cleavage of the proximal cyclopropane bond. Two-thirds of the starting material is incorporated into the zeolite and observed as *tt*-**8**$^{\bullet+}$@HZSM-5. Additional quantities of *tt*-**8** and of its geometric isomer, *ct*-**8**, were isolated from the supernatant solution, further supporting proximal bond cleavage. The third product, **9**, also requires cleavage of the proximal bond and reveals either an additional pathway for the intermediate involved or, alternatively, an additional intermediate.

The structure of the major product, *tt*-**8**$^{\bullet+}$@HZSM-5, rests securely on a comparison of its ESR and DR spectra with those obtained by incorporation of authentic *tt*-**8**.[6a,b] Furthermore, the ESR spectra were in good agreement with those obtained by Ramamurthy et al. upon adsorbing *tt*-**8** onto ZSM-5.[6a] In addition, an ESR spectrum simulated with hfccs calculated for *tt*-**8**$^{\bullet+}$ on the basis of DFT reproduced the experimental spectrum well. The hfcc's shown below reflect the delocalization of unpaired spin density throughout *tt*-**8**$^{\bullet+}$.

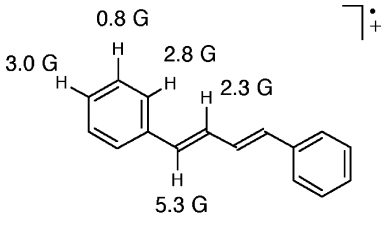

tt-**8**$^{\bullet+}$

(23) Roth, H. D.; Schilling, M. L. M. *J. Am. Chem. Soc.* **1980**, *102*, 7956−7958.
(24) (a) Davies, A. G.; Sutcliffe, R. *J. Chem. Soc., Perkin Trans. 2* **1980**, 819−824. (b) Davies, A. G.; Griller, D.; Ingold, K. U.; Lindsay, D. A.; Walton, J. C. *J. Chem. Soc., Perkin Trans. 2* **1981**, 633−641.

Scheme 6

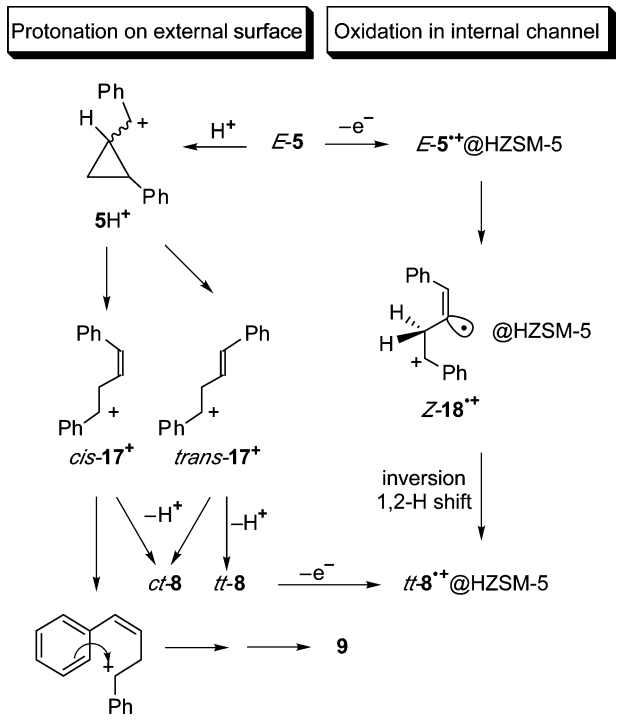

Additionally, the ESR and DR spectra of *tt*-**8**$^{\bullet+}$@HZSM-5 essentially agree with the ESR (Figure 3, bottom) and absorption spectra (Figure 4, top) obtained by γ-irradiation of *tt*-**8** in a glassy matrix of *n*-BuCl at 77 K. The fact that the ESR signals of *tt*-**8**$^{\bullet+}$@HZSM-5 (Figure 3, top) are noticeably sharper than those of *tt*-**8**$^{\bullet+}$ in the frozen matrix (Figure 3, bottom) may be due to a less restricted mobility of the guest in the zeolite or to multiple sites in the glassy matrix. Interestingly, the electronic spectra of *tt*-**8**$^{\bullet+}$ in the two matrices have different maxima: the DR spectrum in the zeolite (540, 817 nm) is slightly blue-shifted compared to the absorption in the matrix (548, 822 nm). This observation may be due to the strong electrostatic fields[25] and/or the electronic confinement[26] in the restrictive zeolite interior.

These experimental results leave little doubt that the proximal bond of *E*-**5** is cleaved inside HZSM-5 or on its surface. Considering the redox activity as well as the Brønsted and Lewis acidities of the external and internal surfaces of HZSM-5, we consider two mechanisms for the conversion of *E*-**5** to *tt*-**8**$^{\bullet+}$@HZSM-5, with two different species as key intermediates (Scheme 6).

The first pathway to be considered is initiated by the oxidation of *E*-**5** molecules that are at least partially immersed in the zeolite interior (cf., Figure 7). The resulting *E*-**5**$^{\bullet+}$@HZSM-5 might cleave the (phenyl-activated) proximal bond, yielding a bifunctional 1,3-radical cation, *Z*-**18**$^{\bullet+}$@HZSM-5, as the crucial intermediate. A subsequent inversion at the vinylic radical center and a 1,2-H shift might convert *Z*-**18**$^{\bullet+}$@HZSM-5 to *tt*-**8**$^{\bullet+}$@HZSM-5. The isomeric product *ct*-**8** can be formed from *Z*-**18**$^{\bullet+}$ by a 1,2-H shift without inversion; however, the formation of **9** cannot be explained readily.

(25) (a) Rabo, J. A.; Angell, C. L.; Kasai, P. H.; Schomaker, V. *Discuss. Faraday Soc.* **1966**, *41*, 328−349. (b) Dempsey, E. *J. Phys. Chem.* **1969**, *73*, 3660−3668. (c) Jousse, F.; Lara, E. C. d. *J. Phys. Chem.* **1966**, *100*, 233−237.
(26) Márquez, F.; García, H.; Palomares, E.; Fernández, L.; Corma, A. *J. Am. Chem. Soc.* **2000**, *122*, 6520−6521.

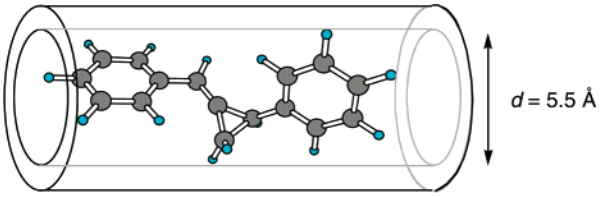

Figure 7. Shape and "width" of *E*-**5**, showing that it is compatible with the HZSM-5 dimension.

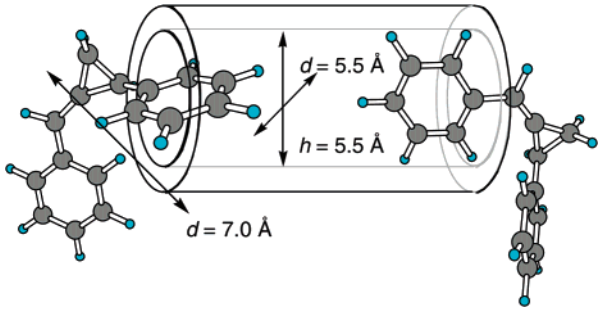

Figure 8. Shape and "width" of *Z*-**5**; the bulk of the *Z*-isomer prevents complete incorporation; either a phenylcyclopropane (left) or a styrene fragment (right) may be incorporated.

The second mechanism involves protonation of *E*-**5**, either inside HZSM-5 or on its surface, forming **5**H$^+$, which would generate *cis*- and *trans*-**17**$^+$ by a cyclopropylcarbinyl rearrangement. Products *ct*-**8** and **9** are then readily explained via *trans*-**17**$^+$ or different rotamers of *cis*-**17**$^+$. Deprotonation of *trans*-**17**$^+$ would yield either *tt*- or *ct*-**8**; deprotonation of *cis*-**17**$^+$ would yield either *ct*- or *cc*-**8**, whereas cyclization followed by a hydrogen shift would generate **9** (Scheme 6). Interestingly, the cyclized product **9** was not observed when adsorbing either *tt*- or *ct*-**8** onto HZSM-5. This finding suggests that product **9** is formed via a reactive intermediate, which is not accessible from *tt*- or *ct*-**8**.

In trying to evaluate the merit of the two mechanisms, we note that the conversion of *E*-**5** to **9** cannot be explained without invoking "special zeolite forces", such as strong electrostatic fields[25] and/or electronic confinement[26] in the zeolite interior; the bifunctional radical cation *Z*-**18**$^{\bullet+}$ does not account readily for the formation of **9**. On the other hand, *cis*-**17**$^+$ appears to be a "natural" intermediate for the formation of **9**. These considerations lead us to conclude that the protonation-induced mechanism is more plausible. This assignment is supported indirectly by the failure of *tt*-**8** to form **9**. Because *tt*-**8** is known to undergo oxidation rather than protonation in HZSM-5,[6a] pathways induced by protonation, i.e., formation of *cis*-**17**$^+$, are precluded.

The protonation-initiated mechanism is further supported by the reactions of two bulkier substrates, the isomer, *Z*-**5**, and the dixylyl derivative, *E*-**11**. The molecular diameters of *Z*-**5** or *E*-**11** ($\sim$7 Å) are larger than the pore size of HZSM-5; the shape of *Z*-**5** allows partial incorporation (either the phenylcyclopropane or the styrene fragment) (Figure 8), whereas *E*-**11** is precluded altogether from entering the HZSM-5 channels. Because the oxidation-initiated mechanism is limited very likely to molecules at least partially immersed into the zeolite interior, *E*-**11** cannot be expected to form any products.

The *Z*-isomer (*Z*-**5**) gave *tt*- and *ct*-**8**, dihydronaphthalene **9**, and the colored *tt*-**8**$^{\bullet+}$@HZSM-5 upon reaction with HZSM-5. These results support the existence of active sites near the

Scheme 7

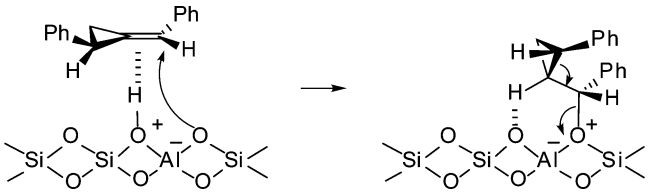

channel entrance or on the external zeolite surface; the formation of **9** must occur outside the zeolite channels, whereas the eventual oxidation to *tt*-**8**$^{\bullet+}$@HZSM-5 requires the complete incorporation of *tt*-**8** into the zeolite channels.

The bulky *E*-**11** gave rise to the respective 1,3-butadienes (*tt*- and *ct*-**12**) and 1,2-dihydronaphthalene derivatives (**13**) but failed to produce coloration on the zeolite surface or any evidence for *tt*-**12**$^{\bullet+}$@HZSM-5. These results support protonation of *E*-**11** on the zeolite exterior and argue against a significant density of redox active sites on the external surface of HZSM-5.

The results observed for *Z*-**5** or *E*-**11** require that the reaction is triggered near the channel entrance or on the external surface of HZSM-5, respectively, most likely via protonation at Brønsted sites such as terminal silanol groups.[27] Although we have no evidence for details, recent studies[28] suggest that the initial protonation may proceed via a π-complex and an alkyl oxonium species (Scheme 7). Product molecules of a suitable shape, viz., *tt*-**8**, can enter the zeolite interior for the oxidation step forming *tt*-**8**$^{\bullet+}$@HZSM-5, either at a Brønsted or a Lewis site (e.g., nonframework AlO^+).[29]

(27) (a) Trombetta, M.; Busca, G. *J. Catal.* **1999**, *187*, 521−523. (b) Trombetta, M.; Armaroli, T.; Alejandre, A. G.; Solis, J. R.; Busca, G. *Appl. Catal., A* **2000**, *192*, 125−136.

(28) (a) Haw, J. F.; Nicholas, J. B.; Xu, T.; Beck, L. W.; Ferguson, D. B. *Acc. Chem. Res.* **1996**, *29*, 259−267. (b) Yang, S.; Kondo, J. N.; Domen, K. *J. Phys. Chem. B* **2001**, *105*, 7878−7881. (c) Kondo, J. N.; Shao, L.; Wakabayashi, F.; Domen, K. *J. Phys. Chem. B* **1997**, *101*, 9314−9320.

(29) (a) Jacobs, P. A.; Beyer, H. K. *J. Phys. Chem.* **1979**, *83*, 1174−1177. (b) Zhang, W.; Han, X.; Liu, X.; Lei, H.; Liu, X.; Bao, X. *Microporous Mesoporous Mater.* **2002**, *53*, 145−152.

Conclusion

We have observed regiodivergent bond cleavage reactions of *E*-**5** by PET reaction in solution and via spontaneous protonation−oxidation by a redox-active acidic zeolite. The PET reaction in solution proceeds by cleavage of the distal cyclopropane bond, whereas the zeolite-induced reaction causes cleavage of the phenyl-activated proximal cyclopropane bond. The results observed for *E*-**5** and for a bulkier analogue, *E*-**11**, provide valuable insight into the mechanism of the zeolite-induced reactions on both the external and internal zeolite surfaces and about the distribution of Lewis and Brønsted acid sites on the zeolite exterior and interior.

Acknowledgment. H.I. and S.T.-K. thank the Ministry of Education, Culture, Sports, Science, and Technology (MEXT) of Japan for financial support in the form of a Grant-in-Aid for Scientific Research in Priority Areas (Area No. 417) and also Professor M. Ueda (Tohoku University) for his generous considerations. K.A. acknowledges financial support from the MEXT of Japan (15350074 and 17651054) and the Core Research for Evolutional Science and Technology of Japan Science and Technology Agency. H.D.R. acknowledges financial support from the National Science Foundation (CHE-9714850). We also acknowledge TOSOH Co. Ltd. for the zeolite samples.

Supporting Information Available: General methods of the experiments, preparation, and isolation of organic materials, evaluation of the electron-accepting ability of zeolites, comparison of ESR spectra of *tt*-**8**$^{\bullet+}$@HZSM-5, and Cartesian coordinates, partial spin, and charge densities of *E*-**10**$^{\bullet+}$ calculated by UB3LYP/6-31G** and UAM1 (PDF). This material is available free of charge via the Internet at http://pubs.acs.org.

JA045930N